Available online at www.sciencedirect.com
ScienceDirect
Atmospheric Environment 41 (2007) 5122–5137
ATMOSPHERIC ENVIRONMENT
www.elsevier.com/locate/atmosenv

Observations of hydroxyl and the sum of peroxy radicals at Summit, Greenland during summer 2003

S.J. Sjostedt[a], L.G. Huey[a,*], D.J. Tanner[a], J. Peischl[a,h], G. Chen[b], J.E. Dibb[c], B. Lefer[d], M.A. Hutterli[e,f], A.J. Beyersdorf[g], N.J. Blake[g], D.R. Blake[g], D. Sueper[h], T. Ryerson[h], J. Burkhart[i], A. Stohl[j]

[a]*School of Earth and Atmospheric Sciences, Georgia Institute of Technology, Atlanta, GA 30332-0340, USA*
[b]*NASA Langley Research Center, Hampton, VA 23681, USA*
[c]*Institute for the Study of Earth, Oceans and Space, University of New Hampshire, Durham, NH 03824-3525, USA*
[d]*Geosciences Department, University of Houston, Houston, TX 77204-5007, USA*
[e]*Department of Hydrology and Water Resources, University of Arizona, Tucson, AZ 85721, USA*
[f]*Physical Sciences Division, British Antarctic Survey, Cambridge, CB3 0ET, UK*
[g]*Department of Chemistry, University of California at Irvine, Irvine, CA 92697-2025, USA*
[h]*NOAA Aeronomy Lab, Boulder, CO 80305-3328, USA*
[i]*School of Engineering, University of California, Merced, Merced, CA 95344-2039, USA*
[j]*Norwegian Institute for Air Research, P.O. Box 100, 2027 Kjeller, Norway*

Received 1 November 2005; received in revised form 12 June 2006; accepted 12 June 2006

Abstract

The first measurements of peroxy ($HO_2 + RO_2$) and hydroxyl (OH) radicals above the arctic snowpack were collected during the summer 2003 campaign at Summit, Greenland. The median measured number densities for peroxy and hydroxyl radicals were 2.2×10^8 mol cm^{-3} and 6.4×10^6 mol cm^{-3}, respectively. The observed peroxy radical values are in excellent agreement ($R^2 = 0.83$, M/O = 1.06) with highly constrained model predictions. However, calculated hydroxyl number densities are consistently more than a factor of 2 lower than the observed values. These results indicate that our current understanding of radical sources and sinks is in accord with our observations in this environment but that there may be a mechanism that is perturbing the ($HO_2 + RO_2$)/OH ratio. This observed ratio was also found to depend on meteorological conditions especially during periods of high winds accompanied by blowing snow. Backward transport model simulations indicate that these periods of high winds were characterized by rapid transport (1–2 days) of marine boundary layer air to Summit. These data suggest that the boundary layer photochemistry at Summit may be periodically impacted by halogens.

Keywords: HO_x; Greenland; Polar; Photochemistry; Hydroxyl radical; Summit

1. Introduction

Over the last decade the chemistry of the polar troposphere has received increased attention

*Corresponding author.
E-mail address: greg.huey@eas.gatech.edu (L.G. Huey).

1352-2310/$ - see front matter © 2007 Published by Elsevier Ltd.
doi:10.1016/j.atmosenv.2006.06.065

(Domine and Shepson, 2002; Davis et al., 2001; Jones et al., 2000; Dibb et al., 2002; Honrath et al., 1999). Previously atmospheric photochemistry in polar regions was expected to be rather inactive since the primary production of hydroxyl radicals (OH) is attenuated at high latitudes due to low dew points and large solar zenith angles. However, a series of recent polar field missions have shown that snowpack can be a source of HO_x (HO_2+OH) precursors (e.g. H_2O_2, CH_2O and HONO) that may significantly enhance production at high latitudes (Honrath et al., 2002; Jacobi et al., 2002; Hutterli et al., 2001, 2004). Furthermore the presence of elevated NO_x ($NO+NO_2$) (Ridley et al., 2000; Honrath et al., 2002; Davis et al., 2001; Jones et al., 2000) can also increase the oxidizing capacity of the polar troposphere by enhancing secondary production of OH through reactions (1) and (2).

$$HO_2 + NO \rightarrow OH + NO_2, \quad (1)$$

$$RO_2 + NO + O_2 \rightarrow R'CHO + HO_2 + NO_2, \quad (2)$$

where $RO_2 = CH_3O_2$, etc.

At the present time there is a limited data set of peroxy and hydroxyl radicals available for the polar boundary layer. Measurements of hydroxyl (Mauldin et al., 2003) and peroxy radicals (Cantrell et al., 2003) have been obtained over the Canadian Arctic during the Tropospheric Ozone Production about the Spring Equinox (TOPSE). Hydroxyl radical concentrations were generally below 3×10^6 mol cm^{-3}; however, the measurements were limited to altitudes above the boundary layer. Peroxy measurements enjoyed greater coverage and were generally between 2 and 3×10^8 mol cm^{-3} from 0.5 to 3 km, the altitude of Summit, during the final (mid-May) deployment. There is a series of hydroxyl (and limited peroxy) radical measurements from the South Pole (SP) by Mauldin et al. (2001, 2004) during the Investigation of Sulfur Chemistry in the Antarctic Troposphere (ISCAT) field campaigns. The daily averaged observed OH number densities during the 1998 and 2000 austral summer ISCAT campaigns were between 2 and 4×10^6 mol cm^{-3}. These results were compared to predictions from a highly constrained photochemical model (Chen et al., 2001). Reasonable agreement between the modeled (M) and observed (O) OH values (median M/O = 1.22) was found at lower NO_x levels (<130 pptv) when snowpack emissions of formaldehyde and hydrogen peroxide were included in the model (Chen et al., 2004). However, constraining the model to observed concentrations of nitrous acid (HONO) led to over predictions by approximately a factor of 3. These results indicated that SP photochemistry is relatively well understood on average but that the importance of HONO as a HO_x precursor is uncertain.

To our knowledge there are no measurements of HO_x radicals above the snowpack in the northern hemisphere. However, there have been a series of campaigns at Summit, Greenland focused on measuring reactive nitrogen and other important photochemical species (e.g. NO_x, HONO, HNO_3, PAN, CH_2O, H_2O_2, etc.) (Hutterli et al., 1999, 2001; Dibb et al., 2002; Jacobi et al., 2002). Hutterli et al. (2001) predicted that hydrogen peroxide and formaldehyde would be responsible for a 70% increase in hydroxyl radicals and a 50% increase in peroxy radicals in the boundary layer. Yang et al. (2002) used the data from the summer 1999 and 2000 Summit campaigns to calculate HO_x number densities with a steady state model. They concluded that HO_x production from precursors such as HONO, H_2O_2 and CH_2O would be of greater magnitude than primary production from ozone photolysis. In the summer 1999 field campaign they predicted that photolysis of formaldehyde would be a stronger HO_x source than photolysis of ozone. Yang et al. (2002) also predicted that during the 2000 field campaign HONO and ozone photolysis sources of HO_x would be of similar magnitude. In both years photolysis of ozone is predicted to be responsible for less than 35% of the total HO_x budget. Yang et al. (2002) also predicted noontime OH concentrations at Summit that are a factor of 2–3 times greater than the observed OH values at the SP. The difference in the predicted Summit OH values relative to the SP is not surprising since primary production rates of HO_x are expected to be higher at Summit due to lower solar zenith angles, higher ozone levels and higher dew points. Chen et al. (2004) predict that ozone photolysis and oxidation of methane are both responsible for 27% of the HO_x budget at the SP with snow sources of formaldehyde (32%) and hydrogen peroxide (14%) providing the remainder. However, secondary production of OH by reactions (1) and (2) at SP is probably much greater than at Summit due to higher NO_x levels (i.e. median SP NO = 225 pptv (Davis et al., 2004), median Summit NO ~15 pptv (Honrath et al., 2002).

In order to probe the photochemistry at Summit, Greenland we made in situ measurements of both

the hydroxyl radical (OH) and the sum of peroxy radicals ($HO_2 + RO_2$) during the Summit 2003 field campaign. In this work we compare these measurements with two highly constrained steady-state models. This analysis provides a test of our understanding of HO_x chemistry in the region where the long glaciochemical records from the Summit ice cores were obtained by the Greenland Ice Sheet Project 2 and the Greenland Ice Core Project (e.g. Hammer et al., 1997; Mayewski and Bender, 1995).

2. Experimental

2.1. Chemical ionization mass spectrometer

The measurements of OH, the sum of $HO_2 + RO_2$ and sulfuric acid were obtained with a chemical ionization mass spectrometer (CIMS). The techniques used for these measurements were based on the work of Tanner et al. (1997) and Edwards et al. (2003). The CIMS consisted of an ambient pressure flow tube reactor and an ion source coupled to a quadrupole mass spectrometer (Fig. 1). The flow reactor is a stainless steel tube approximately 15.3 cm long and 1.25 cm in outer diameter (o.d.) biased at roughly −190 V. Ambient air is transported at 5.0 slpm into this tube from the inlet to the sampling pinhole for the mass spectrometer. The flow reactor is equipped with two sets of opposed injectors, 0.076 cm inner diameter (i.d.) × 0.16 cm o.d. stainless steel tubes, placed approximately 5 cm apart (Fig. 2.). Addition of SO_2 and NO through the front injectors (total flow ~35 sccm) allows for conversion of OH and peroxy radicals to sulfuric acid. Addition of an OH scavenger, hexafluoropropene C_3F_6 (6–12 sccm), through the rear injectors allows termination of the radical chemistry (Dubey et al., 1996).

Ions are produced by a ^{210}Po foil (nominal activity 1.0 mCu) in the annular space between the 1.91 cm o.d. and 2.54 cm o.d. stainless steel tubes. These tubes are concentric with the downstream end of the flow reactor and are held at a potential of −220 V. A flow of 20 slpm filtered ambient air doped with nitric acid and C_3F_6 is maintained in the ion source with a diaphragm pump (KNF-813) and mass flow controller (MKS 1559A). The flow from both the ion source and flow tube is exhausted through another diaphragm pump (GAST DOA-V128) and a second mass flow controller (MKS 1559A). Alpha particles from the polonium foil that interact with the carrier gas form positive ions and thermalized electrons on a short time scale. These electrons initiate formation of $NO_3^- \cdot (HNO_3)_n$ cluster ions by the following reactions (Fehsenfeld et al., 1975):

$$HNO_3 + e^- \rightarrow NO_2^- + OH, \quad (3)$$

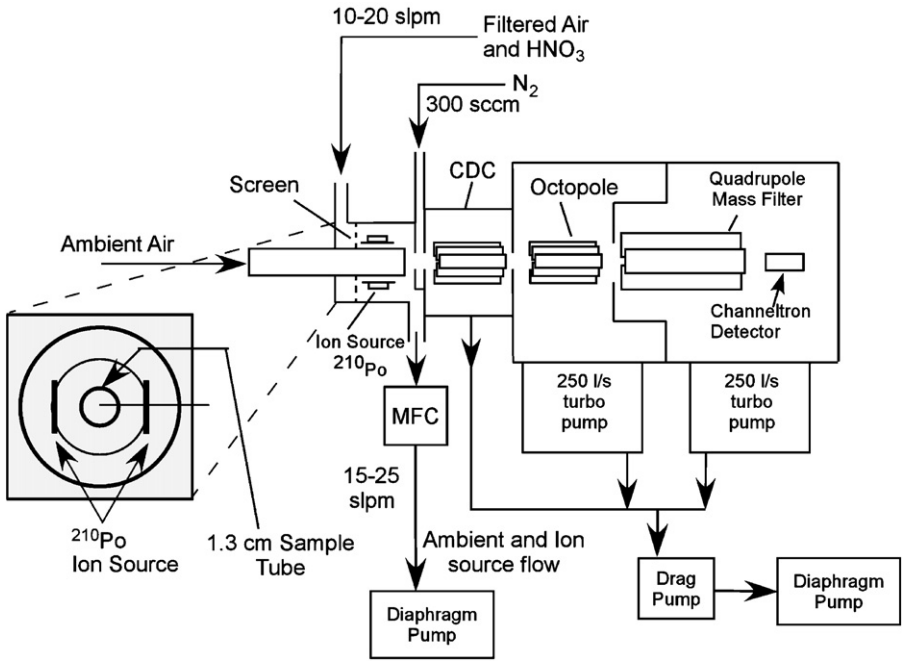

Fig. 1. Schematic of the CIMS used during the Summit 2003 field campaign.

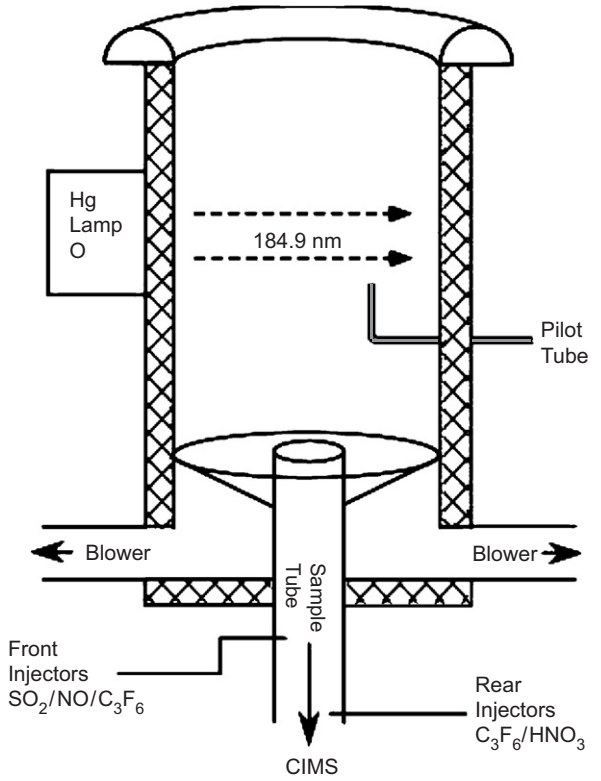

Fig. 2. CIMS inlet configuration. The residence time of the air sample in the inlet is 50 ms.

$$HNO_3 + NO_2^- \rightarrow NO_3^- + HONO, \quad (4)$$

$$HNO_3 + NO_3^- + M \rightarrow NO_3^- \cdot (HNO_3) + M. \quad (5)$$

The nitrate ions from the source react with sulfuric acid by reaction (6) to allow selective detection as HSO_4^- (Viggiano et al., 1982).

$$H_2SO_4 + NO_3^- \cdot (HNO_3) \rightarrow HSO_4^- \cdot (HNO_3) + HNO_3. \quad (6)$$

The potentials of the flow tube and ion source are empirically set to maximize the interaction of the nitrate with the ambient ions exiting the flow tube. This also maximizes the signal levels but does not give excessive mixing of the ambient and ion source flows, which minimizes detection of the OH generated in the ion source by reaction (3). A small portion of the effluent of the flow tube (~150 sccm) is sampled by the mass spectrometer, which is divided into three differentially pumped chambers. The first chamber is a collisional dissociation chamber (CDC) maintained at ~0.4 torr with a drag pump (Alcatel MDP 5011). The CDC is a region of high ion kinetic energy (i.e. high electric field to number density ratio) where cluster ions of nitric acid and/or water are dissociated to simplify the mass spectra.

$$M + HSO_4^- \cdot (HNO_3) \rightarrow HSO_4^- + HNO_3 + M, \quad (7)$$

$$M + HSO_4^- \cdot (H_2O) \rightarrow HSO_4^- + H_2O + M. \quad (8)$$

The second chamber is the octopole ion guide chamber maintained at $\sim 3.0 \times 10^{-3}$ torr by two turbo molecular pumps (Varian 300HT). The octopole transports the ions from the CDC to the final chamber which contains the quadrupole mass filter and detector. The mass selected output of the quadrupole is detected by a channeltron ion multiplier. The pressure of the quadrupole chamber was maintained at $\sim 5.0 \times 10^{-5}$ torr with a third turbo molecular pump (Varian 300HT). The output of the channeltron was amplified and counted as individual ions using standard techniques.

2.2. Conversion chemistry

The nitrate ion chemistry, reaction (6) allows efficient detection of only a few very strong gas phase acids such as sulfuric, methanesulfonic and malonic (Eisele, 1989). Consequently, OH and peroxy radicals are converted to sulfuric acid by reactions (9)–(11) and detected via reaction (6), as described in Eisele and Tanner (1997). Briefly, OH is titrated by an excess of isotopically labeled sulfur dioxide added to the flow tube (10 sccm 0.9% $^{34}SO_2$ in N_2) through the front set of injectors. This initiates the following series of reactions in the sampled air:

$$OH + {}^{34}SO_2 \rightarrow HO^{34}SO_2, \quad (9)$$

$$HO^{34}SO_2 + O_2 \rightarrow HO_2 + {}^{34}SO_3, \quad (10)$$

$${}^{34}SO_3 + 2H_2O \rightarrow H_2{}^{34}SO_4 + H_2O. \quad (11)$$

The use of $^{34}SO_2$ allows simultaneous detection of ambient sulfuric at 97 amu and ambient OH at 99 amu.

Peroxy radicals ($HO_2 + RO_2$) are converted to OH (reactions (1) and (2)) by addition of high levels of NO (10 sccm 0.1% NO in N_2) to the flow tube via the front injectors. The OH is then detected by conversion to H_2SO_4. However, the excess levels of NO can also lead to formation of nitrous acid.

$$OH + NO + M \rightarrow HONO + M. \quad (12)$$

Reaction (12) effectively ties up OH and prevents it from being detected by the CIMS. Consequently,

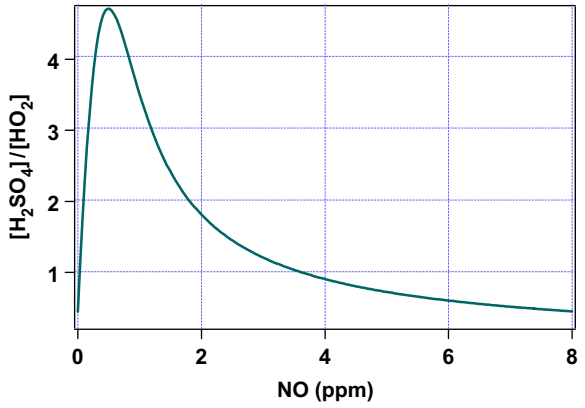

Fig. 3. Predicted yield of sulfuric acid versus nitric oxide mixing ratio at a fixed sulfur dioxide concentration of 32 ppmv. The mixing ratios of NO used during the Summit 2003 field campaign ranged from 3.2 to 6.4 ppmv. The reaction time was 100 ms.

the key parameter for the $HO_2 + RO_2$ measurement is the ratio of [NO] to [SO_2] in the flow tube. In general as the [NO]/[SO_2] increases (above a threshold level) the detection efficiency decreases (Edwards et al., 2003). During the Summit 2003 campaign the [NO]/[SO_2] was set in the range of 0.1–0.2 to achieve a detection efficiency of 1.0–0.5 for $HO_2 + RO_2$. Fig. 3 depicts the predicted H_2SO_4 production from HO_2 as a function of NO addition based on the analytical solution from Edwards et al. (2003).

2.3. CIMS configuration and inlet

The CIMS and all control electronics were deployed in a temperature regulated sheet metal enclosure placed directly on the snowpack (1.0 m deep × 1.1 m wide × 1.5 m high). The CIMS inlet protruded approximately 20 cm through the roof of the enclosure to minimize shading effects. The inlet (Fig. 2) consisted of a 7.6 cm i.d. × 50 cm long aluminum pipe. A flow of approximately 2400 slpm, corresponding to a velocity of $\sim 8\,m\,s^{-1}$, was maintained in the inlet with a regenerative blower. The CIMS flow tube was mounted near the downstream end of the inlet in the center of a turbulence reducing screen. A pitot tube was positioned just off the axis of the inlet to continuously monitor the flow velocity. A temperature controlled mercury lamp (Omega Optical) equipped with a 185 nm bandpass filter was mounted in the wall of the pipe to serve as the calibration source of OH and HO_2 radicals (see below).

The configuration of the CIMS in the heated enclosure was designed for unattended operation of the instrument for most of the campaign. However, two significant problems were encountered with the experimental design. The first of these was observed during the initial measurement period which was characterized by calm winds and clear skies. These conditions gave rise to significant solar heating of the enclosure including the downstream end of the inlet and the flow tube. As a result the conversion efficiency of SO_3 to H_2SO_4, reaction (11), was attenuated due to the strong negative temperature dependence of the reaction of SO_3 with H_2O (Lovejoy et al., 1996). This difficulty was overcome by insulating the inlet and the flow tube from the interior of the enclosure. The second problem was the formation of rime ice on both the inlet screen and flow tube. This primarily occurred during calm evenings when radiation fog was formed. An automated solution for this problem was not found which necessitated frequent cleanings.

2.4. Measurement cycles: calibration and background

Data were collected on a ~7 s cycle, stepping through the reagent ion (NO_3^- = 62 amu) and the product ions (HSO_4^- = 97 amu, $H^{34}SO_4^-$ = 99 amu). A 20 min duty cycle was established for radical measurement (see Fig. 4). For the first 3 min of the measurement cycle NO is added from the front injectors to cycle the peroxy radicals to OH. To determine the background C_3F_6 is added through the front injectors for 90 s every 5 min. The background measurement is triggered halfway through the NO injection to provide a peroxy radical background. In the absence of C_3F_6 and/or NO a mixture of SO_2 and N_2 flows through the front injectors to measure OH. A complication arose from the time required to turn off the NO flow through the injector. This perturbed the first OH measurement period after a $HO_2 + RO_2$ cycle. Therefore these points were excluded from the data set and only the last two OH measurement periods were reported (Fig. 4). Calibration of the OH and peroxy signal is achieved by photolysis of water by 185 nm light generated by a mercury lamp (Tanner et al., 1997).

$$H_2O + h\nu + O_2 \rightarrow OH + HO_2. \quad (13)$$

Since photolysis of water forms both an OH and HO_2 radical the ratio of signal enhancement of

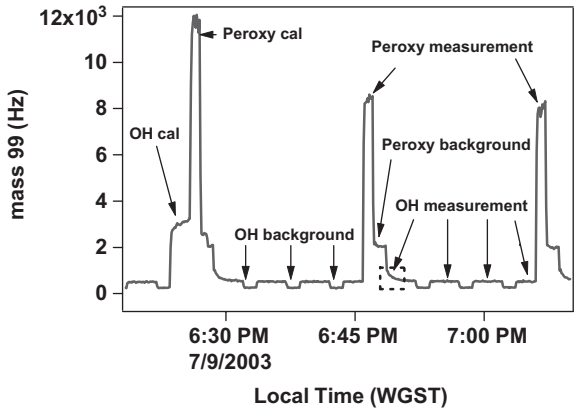

Fig. 4. A typical sequence with measurement, calibration and background periods for hydroxyl and peroxy radicals. The region inside the dashed box is an example of a hydroxyl measurement that is discarded due to lingering NO in the sample tube.

$HO_2 + RO_2$ to OH due to calibration should be 1:1. Deviation from this ratio is used to empirically determine the NO over/under cycling of the observed peroxy signal (Fig. 3). Calibrations were obtained for 5 min every 2 h.

2.5. Accuracy and limit of detection

The accuracy of the measurement depends on the uncertainty inherent in the absorption cross-section of water at 184.9 nm, the response of the photodiodes used to measure the photon flux, the velocity measured inside the inlet and the water concentration obtained from the dew point monitor. The absorption cross-section is known within 5% (Cantrell et al., 1997). The accuracy of the dew point monitor (see below) is 1 °C between −10 and −40 °C. This translates into an uncertainty of 20% in measured H_2O concentration. The uncertainty inherent in obtaining the photon flux is estimated at 12% and the velocity of the inlet was known within 2%. The statistical error (standard deviation) at the 3σ level for the OH calibration signal was typically 9%. This gives a total estimated uncertainty for the CIMS OH measurement of ~25%. There is an additional 3σ statistical error of 25% attributed to the peroxy measurement. The total estimated uncertainty for the peroxy measurement is ~37%. Table 1 provides a summary of the measurement uncertainties. The limit of detection for OH was approximately 1.3×10^5 mol cm^{-3} for a 10 min integration and was estimated as three standard deviations of the background measurement.

Table 1
Summary of the uncertainties in the CIMS measurement

Uncertainty in the peroxy and hydroxyl measurements	
Absorption cross-section of H_2O at 184.9 nm	5%
Photon flux (diodes)	12%
Inlet velocity (pitot tube)	2%
[H_2O] Dew point meter	20%
3σ statistical error for OH calibration	9%
3σ statistical error for the peroxy calibration	25%

2.6. Additional measurements

Measurements of NO, ozone, water vapor, HONO, HNO_3, H_2O_2, CH_2O and actinic flux were all obtained within 5 m of the CIMS instrument. Water vapor and ozone concentrations were measured with commercial instruments (Vaisala HMM 211 and Thermo Environmental Model 49). NO mixing ratios were obtained from a chemiluminescence detector nearly identical to that described by Ryerson et al. (2000). Photodissociation rates were calculated from data gathered from a Scanning Actinic Flux Spectroradiometer (Shetter and Müller, 1999). Nitrous and nitric acid were sampled by a mist chamber coupled with an ion chromatograph as described by Dibb et al. (1998). Hydrogen peroxide and formaldehyde were quantitatively scrubbed from the air into a water stream and then fluorometrically detected in the liquid phase (Hutterli et al., 2004). Volatile organic compounds including carbon monoxide and methane were measured in whole air samples collected at Summit in steel canisters pressurized with a metal bellows pump (Swanson et al., 2002).

2.7. Photochemical models

Number densities of OH, HO_2, NO_2 and various RO_2 species (e.g. CH_3O_2) were calculated with a steady-state box model that utilized explicit HO_x–NO_x–CH_4 chemistry (71 reactions). The model incorporates a parameterized chemical scheme (184 reactions) to describe the non-methane hydrocarbon (NMHC) oxidations (Chen et al., 2004). The model calculations were constrained by observations of a suite of chemical species, including HO_x precursors H_2O_2 and CH_2O, photolysis rates and NMHC of which ethane and propane were the two dominant species. Model runs were also performed with and without HONO to assess its impact on the HO_x budget. All model calculations were performed on a 10 min data merge. Model runs constrained by

HONO are limited by availability of measurements (generally after 8:00 AM local time). Model runs without HONO were run 24 h a day excluding periods of missing radical or precursor data. A simpler model utilizing explicit HO_x-NO_x-CH_4 (30 reactions) similar to the mechanism described in Chen et al. (2001) was used to check the contribution of NMHC. Predicted number densities of hydroxyl radicals were ~8% lower when the NMHC model was used while predicted peroxy number densities were 3% higher. The model using NMHC will be the model referenced for the duration of the paper.

Two filters were applied to the data to remove invalid or questionable data points. No levels above 100 pptv were discarded to discriminate against pollution from the station generator. The pollution (high NO_x) events were also accompanied by light winds from the north to northeast. The second filter was for wind speeds above $6\,m\,s^{-1}$. This filter was applied as higher wind speeds were found to increase the uncertainty in the instrument calibration as well as to decrease the sensitivity of the instrument. In addition, this filter also allowed us to separate out the periods of blowing snow which exhibited HO_x chemistry that was very different than observed during calm periods (see Results). Except for the time series and the high wind case study, the high wind data were excluded from model comparisons and reported averages due to a possible positive experimental artifact (see Discussion).

2.8. Air mass characterization

The Lagrangian particle dispersion model FLEXPART was used to determine the source region of air impacting Summit. FLEXPART is a particle dispersion model with full turbulence and convection parameterizations (Stohl et al., 2005) and for this study was run backward in time from the Summit site. The theory underlying the backward calculations is presented by Seibert and Frank (2004), and applications to aircraft measurements were presented by Stohl et al. (2003). Backward simulations are presented for the high wind event (28 June) and representative low wind day (9 July). The model output consists of mapped emission sensitivities, which are proportional to residence times of the particles and, for the purpose of this study, can be interpreted in a similar way as simple back trajectory calculations.

3. Results and analysis

3.1. Peroxy radicals ($HO_2 + RO_2$)

The median measured $HO_2 + RO_2$ number density for the entire mission was $2.2 \times 10^8\,mol\,cm^{-3}$ (mean $2.4 \times 10^8\,mol\,cm^{-3}$). During the observation period with concurrent HONO measurements the median number density for $HO_2 + RO_2$ was $3.4 \times 10^8\,mol\,cm^{-3}$. The HONO measurement coverage excludes ~25% of the HO_x measurements. Median noontime, 10:00 AM–3:00 PM West Greenland Summer Time (WGST = UTC−2 h), values for peroxy radicals were $4.1 \times 10^8\,mol\,cm^{-3}$. A comparison of measured and modeled (without HONO) peroxy radical number densities is presented in Fig. 5. These data have been filtered for station pollution but not for high winds. Wind speed has also been included to demonstrate the correlation between high winds and the periods of greatest divergence between the measured and modeled values.

Two model runs were compared to observations (Fig. 6). In the first run the model was constrained to all measured precursors (solid black diamonds) and in the second run measured HONO was excluded from the model (open green diamonds). Model predictions for $HO_2 + RO_2$ are in excellent agreement ($R^2 = 0.83$, see Fig. 6) with observed peroxy values when constrained to H_2O_2 and CH_2O observations and for wind velocities less than $6\,m\,s^{-1}$. Even when peroxy radical measurements at high wind speeds are included the correlation is still robust ($R^2 = 0.75$). The median ratio of modeled to observed (M/O) for peroxy radicals is 1.06 for the filtered data set. When HONO is added as a constraint to the model the M/O ratio increases by ~20% for peroxy radicals.

Finally the observations and model prediction (with HONO) for the entire field campaign were averaged into a composite 24 h 'day' with 10 min time resolution, shown in Fig. 7. The correlation between the binned observations and the model is excellent (R^2 of 0.88) with a median M/O of 1.16. Slightly better results are obtained when comparing the binned data not constrained to observed HONO with a median M/O of 1.01

3.2. Hydroxyl radicals (OH)

The median observed OH number density was $6.4 \times 10^6\,mol\,cm^{-3}$ (mean $6.3 \times 10^6\,mol\,cm^{-3}$)

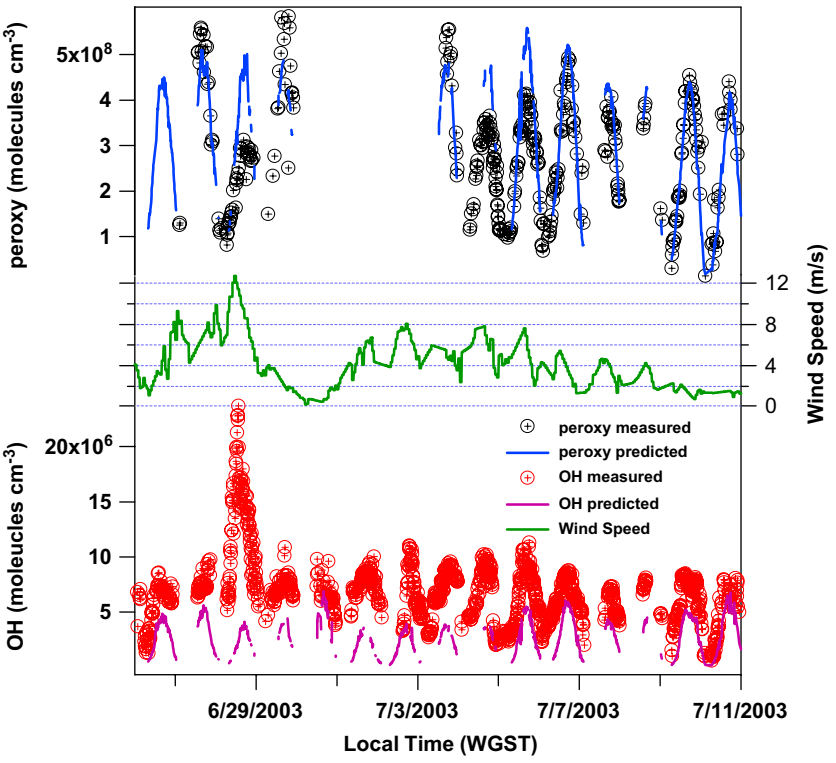

Fig. 5. Time series of hydroxyl and peroxy radical measurements and wind speed. The black circles and the solid blue line represent measured and modeled peroxy concentrations. The red circles and solid purple line represent measured and modeled hydroxyl concentrations. The green line indicates wind speed. Note that the gap in peroxy radical measurement was due to removal of the NO addition. This was done to make sure that a possible NO leak in the sample tube did not lead to high measurements of hydroxyl radicals.

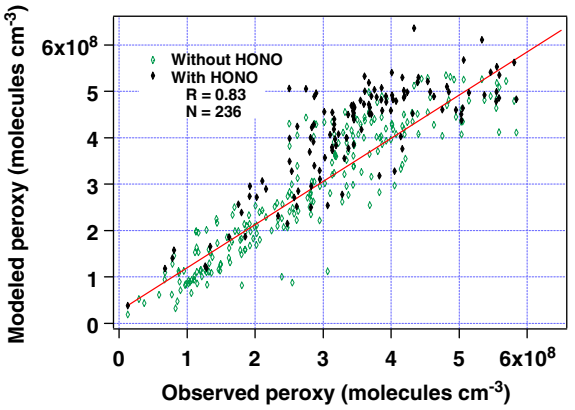

Fig. 6. Scatter plot of predicted versus measured $HO_2 + RO_2$ radicals. Model results without HONO are represented by open green diamonds and results with HONO are indicated by solid black diamonds. The linear regression is fit to model results without HONO.

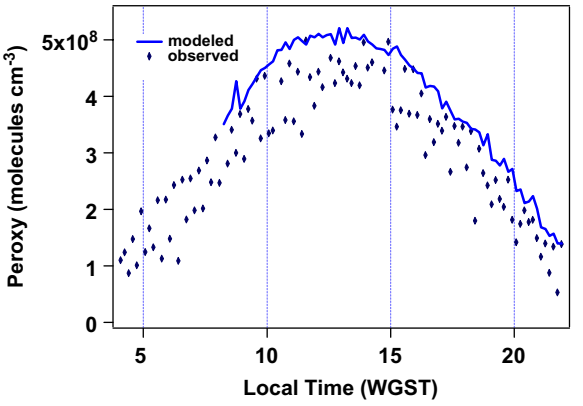

Fig. 7. Composite 24 h measurements and model predictions of peroxy radicals. Predicted values obtained from NMHC model constrained by H_2O_2, CH_2O and HONO.

for the entire mission. The median OH during periods of concurrent HONO measurements is 7.7×10^6 mol cm^{-3} and the noontime median OH concentration was 8.4×10^6 mol cm^{-3}. The agreement between OH measurements and model predictions was not as good as for the peroxy radicals. Measured values were typically a factor of 2–3 higher than the predicted values. The discrepancy

between the model and measured values was found to depend strongly on meteorology. This is depicted in the time series presented in Fig. 5. During the periods of high wind and blowing snow ($>6\,m\,s^{-1}$) highly elevated concentrations of OH were routinely observed (see below and Fig. 5). However, during clear periods with light winds model predictions and observations were in better agreement. The longest such period, was between 8 July and 11 July. During this time a reasonable correlation ($R^2 = 0.47$) and median M/O (0.65) were found when the model was constrained by HONO (Fig. 8). When the model was not constrained by HONO the correlation improved ($R^2 = 0.77$) while the median M/O dropped to 0.48. However, much of the improvement in the correlation can be attributed to greater data coverage when the comparison is not limited to the HONO data set.

The correlation between the low wind speed, binned 10 min modeled and measured OH is strong (R^2 of 0.83, Fig. 9). However, even with this extensive data selection the model still under-predicts the OH concentration by a factor of 2 when constrained to HONO. This indicates that the predicted ratio of peroxy radicals to hydroxyl radicals (($HO_2 + RO_2$/OH) is too high. The median predicted ($HO_2 + RO_2$)/OH for the low wind data is 115:1 and is essentially independent of HONO, by comparison the median measured ($HO_2 + RO_2$)/OH is 45:1.

3.3. Case studies—high and low wind

As mentioned above meteorological conditions appear to play a role in the radical concentrations.

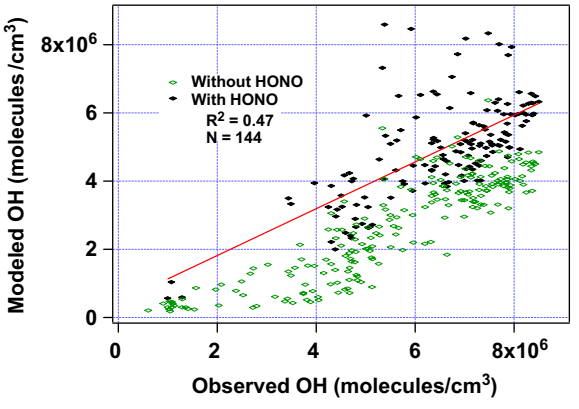

Fig. 8. Scatter plot of predicted versus measured OH radicals for the last four days of the field campaign (7/8–7/11, 2003). Model results without HONO are represented by open green diamonds and results with HONO are indicated by solid black diamonds. The linear regression is fit to model results with HONO.

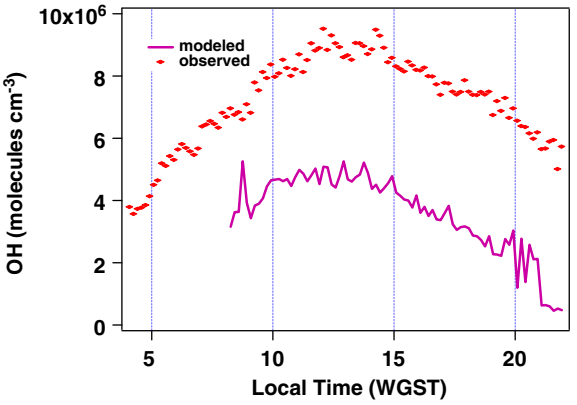

Fig. 9. Composite 24 h measurements and model predictions of OH. Predicted values obtained from NMHC model constrained by H_2O_2, CH_2O and HONO.

For this reason, data from 9 July and 28 June are shown in more detail to illustrate data from meteorological extremes. 9 July (Fig. 10) was a clear day with light winds (mean $= 1.6\,m\,s^{-1}$) and an average temperature of $-17.6\,^{\circ}C$. The median number density for OH was $5.6 \times 10^6\,mol\,cm^{-3}$ and $2.5 \times 10^8\,mol\,cm^{-3}$ for $HO_2 + RO_2$ with a corresponding ($HO_2 + RO_2$)/OH ratio of 45:1. At midday (10:00 AM–3:00 PM WGST) OH production was $3.8 \times 10^6\,mol\,cm^{-3}\,s^{-1}$ and HO_x production was $2.0 \times 10^6\,mol\,cm^{-3}\,s^{-1}$. OH production was a factor of 2 larger than HO_x production because the cycling of HO_2 to OH by NO (reaction (1)) was calculated to be the dominant source of hydroxyl radicals on this date. The mean midday NO mixing ratio was 28 pptv and the predicted ($HO_2 + RO_2$)/OH ratio was 83:1. Observed midday OH and $HO_2 + RO_2$ number densities were 7.7×10^6 and 4.3×10^8, respectively, which led to a ($HO_2 + RO_2$)/OH ratio of 56:1. Ozone remained fairly constant (50 ppb) throughout the measurement period dropping down to a minimum of 47.5 ppb late in the day. Backward simulations derived from the FLEXPART model (Fig. 11) indicate that majority of the air sampled at Summit had been lingering over the Greenland ice sheet for several days and was mainly from high altitudes with little time spent in the boundary layer.

In contrast 28 June (Fig. 12) was a warm day (average temperature = $-12.4\,C$) with strong advection from the south accompanied by heavy blowing/falling snow. Visibility was frequently less than 10 m. The median OH concentration was $1.1 \times 10^7\,mol\,cm^{-3}$, the highest daily average for the mission, while the peroxy number density was a

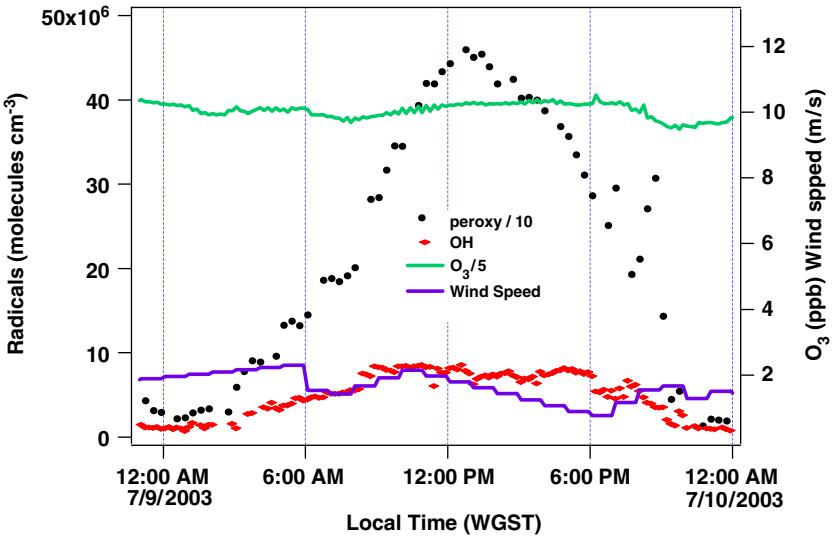

Fig. 10. Measured values for radicals, ozone and wind speed on 9 July. Black dots = peroxy radicals (number density/10), red diamonds = OH (number density), green line = ozone (ppbv/5) and blue Line = wind speed ($m\,s^{-1}$).

relatively modest $2.1\times10^{8}\,mol\,cm^{-3}$. The daily $(HO_2+RO_2)/OH$ ratio was 19:1. By comparison the midday OH and HO_x rates of production were 2.8×10^{6} and $2.1\times10^{6}\,mol\,cm^{-3}\,s^{-1}$, respectively. The NO midday mixing ratio was 9 pptv. The predicted midday $(HO_2+RO_2)/OH$ ratio was 128:1 or a factor of 7 increase over the observed ratio. The period between 8:00–10:00 AM further illustrates this point. During this period the wind speed achieved a maximum of $12\,m\,s^{-1}$ and was accompanied by the daytime minimum mixing ratio of ozone (44 ppbv). The measured OH number densities climbed to $2.0\times10^{7}\,mol\,cm^{-3}$ during this event and the ratio of $(HO_2+RO_2)/OH$ dropped to 10:1. The modeled $(HO_2+RO_2)/OH$ during the high wind event was 143:1 or a 14 fold increase over the observed ratio. In addition the largest disagreement between modeled and observed HO_2+RO_2 is observed during this time. The FLEXPART backwards simulations (Fig. 13) show that the air sampled at Summit on 28 June was influenced by a low pressure system in the Irminger Sea. Retroplume analysis indicates that the majority of the Summit air mass had been located over the ocean recently (1–2 days) with a large component from the boundary layer. These data suggest that during these extreme conditions that there is either a positive experimental artifact in the OH or that there is unidentified chemistry that significantly perturbs the $(HO_2+RO_2)/OH$ ratio associated with blowing snow or marine air masses.

4. Discussion

The excellent agreement between measured and modeled peroxy radical number densities suggests that HO_x sources and sinks at Summit are relatively well understood. On average the largest source in the HO_x budget is photolysis of O_3 (~40%), followed by the photolysis of H_2O_2 (~30%), photolysis of HONO (~22%) and photolysis of CH_2O (~8%) when the model is constrained by HONO. When the model is not constrained to HONO it lowers the predicted values for peroxy and hydroxyl radicals by ~20%, which is similar in magnitude to the uncertainty of the photolysis rate of HONO (Stutz et al., 2000). By comparison the SP model runs constrained with observed HONO values were entirely inconsistent with measured OH values. This led to speculation by Chen et al. (2004) that the HONO mist chamber values might be due to some interfering species. The lower impact of HONO at Summit relative to the SP is a function of both lower mixing ratios, SP median = 33 ppt (Dibb et al., 2004), Summit median = 10 ppt (Dibb, this issue) and higher radical production from ozone and hydrogen peroxide. Consequently, the Summit 2003 data do not provide a good test of the validity of measured HONO values. However, the data clearly indicate that HONO is not the dominant HO_x source at Summit in the summer of 2003.

Inclusion of HONO does improve the modeled to observed ratio for OH. Over the entire mission

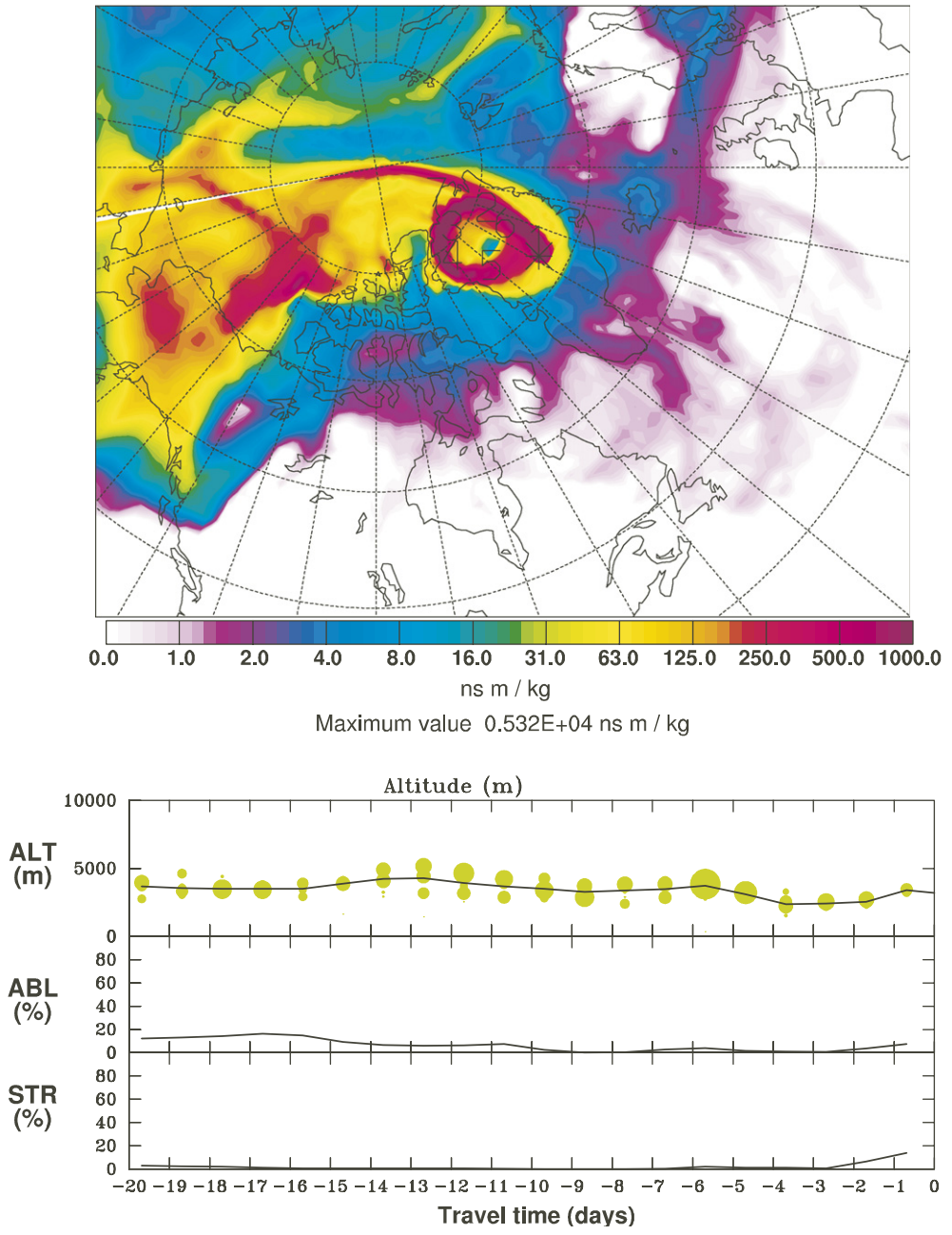

Fig. 11. FLEXPART 20-day model back projection for 9 July. The emission sensitivity integrated over the entire atmospheric column (at the top) indicates that the majority of the air sampled at Summit was from the surrounding Greenland Ice cap. The altitude profile reinforces this conclusion and indicates that the air spent little time in the boundary layer. This was confirmed by low values of the emission sensitivity for the lowest 100 m of the atmosphere (not shown).

(without filter for high wind) the median M/O increases from 0.39 to 0.45 when the model is constrained to HONO. The improvement is even more dramatic during the last four days of the mission, an extended period of calm winds and clear skies, when the median M/O improves from 0.47 to 0.65 with HONO. This ~35% underestimation "best case" scenario is of the order of the uncertainty in the measurement. However, the inclusion of HONO does not improve the

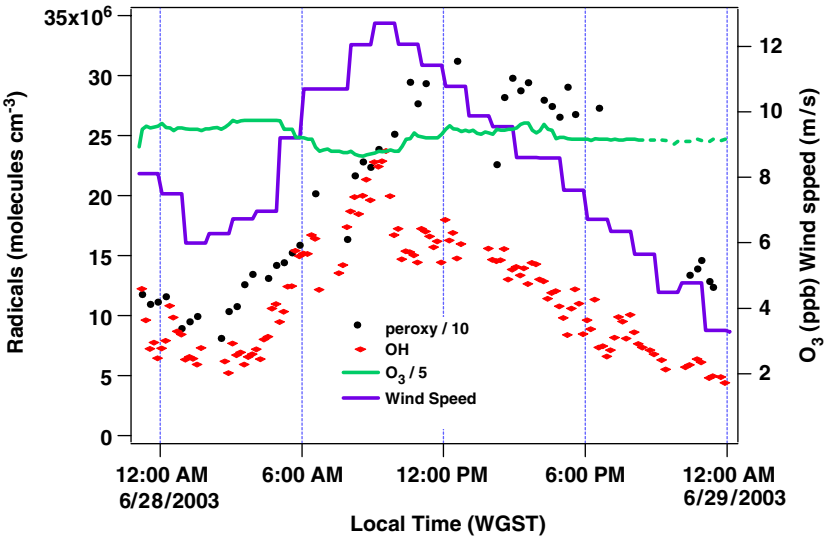

Fig. 12. Measured values for radicals, ozone and wind speed on 28 June. Black dots = peroxy radicals (number density/10), red diamonds = OH (number density), green line = ozone (ppbv/5) and blue line = wind speed ($m\,s^{-1}$).

agreement between the predicted and measured ratio of $(HO_2 + RO_2)/OH$. In addition during periods of highest winds ($>10\,m\,s^{-1}$) the measured values of OH were an order of magnitude larger than predicted. An experimental artifact in high winds and blowing snow would provide a simple explanation to this observation. However, characterization of the instrument indicates that the instrument only loses sensitivity to OH during periods of high crosswinds.

The measured OH values compare reasonably well with the predicted noontime values of OH in Yang et al. (2002), but the measured peroxy values are a factor of 2 less than their predicted values. It should be noted that the measurements and their model predictions are for two different years and the models used in the present work are constrained by a greater suite of measured values. For this reason, we performed model calculations (without NMHC) constrained to 1999 values for the input parameters (H_2O, NO, O_3, HONO, CH_2O, H_2O_2, CO, CH_4, *j*-values) used in the Yang model. We calculate an OH number density of $4.7 \times 10^6\,mol\,cm^{-3}$ and a peroxy radical number density of $4.4 \times 10^8\,mol\,cm^{-3}$. Both are roughly a factor of 2 less than the values predicted by Yang et al. (2002). There are also differences in the relative magnitude of HO_x sources between the two models. This disagreement between the two models does vary to some extent with the value of the parameter α ($\alpha = [HO_2]/[HO_2] + [CH_3O_2]$) that is used to constrain the Yang model. The models used in this work do not use this parameter but instead explicitly calculate peroxy radical concentrations from the mechanism. This difference between the calculations is a likely source of the discrepancy between the results.

Since measured peroxy radical levels are well reproduced by model calculations, ozone production rates ($PO_3 = k_1[RO_2][NO] + k_2[HO_2][NO]$) should be accurately predicted. During the 2003 Summit field campaign average production rates of $\sim 0.8\,ppbv\,day^{-1}$ were calculated for the boundary layer, which is about 2% of the daily average ozone mixing ratio. However, at Summit surface layer photochemical production does not appear to influence ozone levels (Helmig et al., this issue). In fact the boundary layer appears to be slightly depleted in ozone as balloon profiles frequently show higher mixing ratios above the boundary layer (Helmig et al., 2002). In addition firn air measurements of ozone at Summit are lower than ambient, often by a factor of 2 or more (Peterson and Honrath, 2001). The difference between ambient and firn measurements is greatest during the day implying photochemical loss in the interstitial air (Peterson and Honrath, 2001).

These observations are not in accord with those at the SP, where an average boundary layer production of $\sim$2–4 $ppbv\,day^{-1}$ is predicted

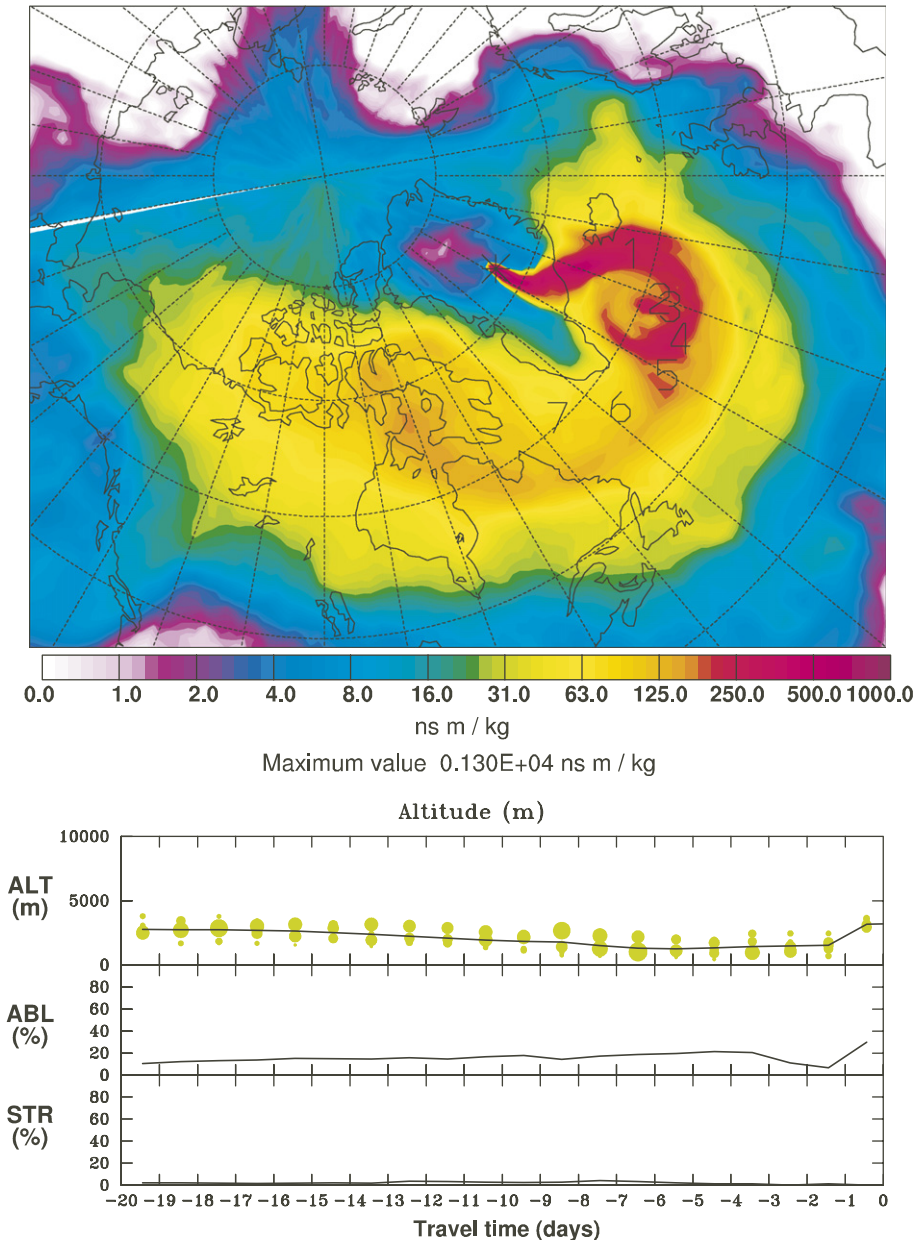

Fig. 13. FLEXPART model 20-day back projection for 28 June. The emission sensitivity integrated over the entire atmospheric (at the top) indicates that there was a strong flow of marine air to Summit from a low pressure system in the North Atlantic. Numbers mark the average position of the air mass at daily intervals back in time and show that the air was already south of Iceland one day previously. A marine boundary layer origin is also suggested by the low average altitude of the tracked particles (lower panel) and the significant percentage of atmospheric boundary layer air (ABL). Plots of the emission sensitivity for the lowest 100 m of the atmosphere (not shown) also reveal high values over the North Atlantic Ocean.

(Chen et al., 2004) The SP ozone record displays photochemical production during early summer that is superimposed on the summer minimum in average ozone levels (Crawford et al., 2001). Balloon measurements of ozone at the SP also show an enhancement of ozone in the boundary layer (Helmig et al. in review) and destruction in the firn air is of lesser magnitude than what is observed at Summit.

Data from ISCAT 2000 indicate a depletion of ~20% (Davis et al., unpublished results).

We speculate that the lack of observed ozone production at Summit and the perturbed $(HO_2+RO_2)/OH$ ratio might be explained by a similar chemical mechanism. The presence of halogen radicals could help explain both the slight depletion of boundary layer ozone and the enhancement in OH (Foster et al., 2001; von Glasow et al., 2004; Stutz et al., 1999). At coastal Arctic sites increases in bromine oxide (BrO) have been well documented during ozone depletion events (Barrie et al., 1988; Hausmann and Platt, 1994; Hönninger and Platt, 2002). It is also possible that this chemistry could be altered by heterogeneous processes due to increased surface area (blowing snow) in the high wind events. Alternatively, rapid transport of air from the marine boundary layer (as suggested by FLEXPART backwards simulations) to Summit might be another mechanism for activating halogen chemistry.

The connection between HO_x chemistry and halogen oxides has been recently investigated in coastal environments. Measurements of HO_x, BrO and IO were obtained at Mace Head, Ireland during the NAMBLEX field campaign (Bloss et al., 2005; Smith et al., 2005; Sommarvia et al., 2005). Daily maximum mixing ratios of IO were between 0.8 and 4.0 pptv (Bloss et al., 2005) and BrO levels were measured up to 6.5 pptv (Saiz-Lopex et al., 2004). In this coastal environment photolysis of HOI was calculated to be responsible for 15% OH production and photolysis of HOBr was estimated to be of similar magnitude. These results demonstrate that halogens could significantly impact the HO_2+RO_2 to OH ratio through photolysis of HOI and/or HOBr.

Although there are no measurements of BrO or IO at Summit there exists ancillary evidence that suggests that both species may be present. Low concentrations (1–2 pptv) of soluble gas phase bromide were consistently detected by the UNH mist chamber during the summer 2003 mission (Evans et al., 2003). However, on 28 June soluble gas phase bromide was above 8 pptv from the onset of measurement (10:00 AM WGST) until 2:30 PM WGST and reached a maximum of 11 pptv during this period. Halocarbons such as methyl bromide, ethyl bromide, methyl iodide and ethyl iodide have been observed in the atmosphere at Summit (Swanson et al., 2002). The observed concentrations of all four are enhanced in the firn column indicating active photochemistry involving halogen radicals within the snowpack (A. Swanson, private communication). Annual changes of iso-butane/propane ratios in the firn column at Summit also suggest a seasonal variance of bromine radicals. Consequently, we believe that further study of photochemistry at Summit should address the potential link between HO_x and halogen chemistry in this environment by direct measurement of such species as BrO.

5. Summary

The excellent agreement between modeled and observed values for HO_2+RO_2 indicates a good understanding of radical sources and sinks at Summit. The OH modeled to observed comparison is not as good, but improves substantially when filtered for high winds and averaged over the duration of the mission into a 24 h composite day. However, the model still under-predicts the observed OH levels by a factor of 2. Hydroxyl radical observations are much higher than model predictions during periods of high winds and blowing snow and rapid transport of marine air to Summit. This indicates that these conditions either produce an artifact within the CIMS or lead to enhanced OH partitioning. We suggest that low levels of BrO and/or IO could explain the observed $(HO_2+RO_2)/OH$ ratio to a significant extent. Inclusion of HONO does improve the agreement between measured and modeled OH, but does not improve the agreement between the predicted and observed $(HO_2+RO_2)/OH$ ratio. The impact of HONO on HO_x levels is less than 20% on average which is well within the uncertainty of the measurements alone. For this reason, the importance of HONO as a radical source in polar environments is not fully elucidated by this data set.

Acknowledgments

This field campaign was made possible by NSF Grant 0220862 through the Office of Polar Programs. We would like to thank VECO Polar Resources (VPR) for logistical support, the Air National Guard 109th for transportation and the support of Greenland home rule. Thanks are also due to Konrad Steffen for meteorological data incorporated in model predictions. Finally, we would like to recognize Sarah Goodwin for her assistance with data acquisition.

References

Barrie, L.A., Bottenheim, J.W., Schnell, R.C., Crutzen, P.J., Rasmussen, R.A., 1988. Ozone destruction and photochemical reactions at polar sunrise in the lower Arctic atmosphere. Nature 334, 138–141.

Bloss, W.J., Lee, J.D., Johnson, G.P., Sommariva, R., Heard, D.E., Saiz-Lopez, A., Plane, J.M.C., McFiggans, G., Coe, H., Flynn, M., Williams, P., Rickard, A.R., Fleming, Z.L., 2005. Impact of halogen monoxide chemistry upon boundary layer OH and HO_2 concentrations at a coastal site. Geophysical Research Letters 32, 6814–6817.

Cantrell, C.A., Zimmer, A., Tyndall, G.S., 1997. Absorption cross sections for water vapor from 183 nm to 193 nm. Geophysical Research Letters 24, 2195–2198.

Cantrell, C.A., Edwards, G.D., Stephens, S., Mauldin, L., Kosciuch, E., Zondlo, M., Eisele, F., 2003. Peroxy radical measurements using chemical ionization mass spectrometry during TOPSE. Journal of Geophysical Research 108, 8371–8385.

Chen, G., Davis, D.D., Crawford, J., Nowak, J.B., Eisele, F., Mauldin, R.L., Tanner, D., Buhr, M., Shetter, R., Lefer, B., Arimoto, R., Hogan, A., Blake, D., 2001. An investigation of South Pole HO_x chemistry: comparison of model results with ISCAT observations. Geophysical Research Letters 28, 3633–3636.

Chen, G., Davis, D., Crawford, J., Mauldin, L., Eisele, F., Huey, G., Slusher, D., Tanner, D.J., Dibb, J., Buhr, M., Hutterli, M.A., McConnell, J., Lefer, B., Shetter, R., Blake, D., Lombardi, K., Arnoldy, J., 2004. A reassessment of HO_x chemistry based on observations recorded during ISCAT 2000. Atmospheric Environment 38, 5451–5462.

Crawford, J.H., Davis, D.D., Chen, G., Buhr, M., Oltmans, S., Weller, R., Mauldin, L., Eisele, F., Shetter, R., Lefer, B., Arimoto, R., Hogan, A, 2001. Evidence for photochemical production of ozone at the South Pole surface. Geophysical Research Letters 28, 3641–3644.

Davis, D., Nowak, J.B., Chen, G., Buhr, M., Arimoto, R., Hogan, A., Eisele, F., Mauldin, L., Tanner, D., Shetter, R., Lefer, B., McMurry, P., 2001. Unexpected high levels of NO observed at South Pole. Geophysical Research Letters 28, 3625–3628.

Dibb, J.E., Talbot, R.W., Munger, J.W., Jacob, D.J., Fan, S.-M., 1998. Air–snow exchange of HNO3 and NO_y at Summit, Greenland. Journal of Geophysical Research 103, 3475–3486.

Dibb, J.E., Arsenault, M., Peterson, M.C., Honrath, R.E., 2002. Fast nitrogen oxide photochemistry in Summit, Greenland snow. Atmospheric Environment 36, 2501–2511.

Dibb, J.E., Huey, L.G., Slusher, D.L., Tanner, D.J., 2004. Soluble reactive nitrogen oxides at South Pole during ISCAT 2000. Atmospheric Environment 38, 5399–5409.

Domine, F., Shepson, P.B., 2002. Air–snow interactions and atmospheric chemistry. Science 297 (5586), 1506–1510.

Dubey, M.K., Hanisco, T.F., Wennberg, P.O., Anderson, J.G., 1996. Monitoring potential photochemical interference in laser induced fluorescence measurements of atmospheric OH. Geophysical Research Letters 23, 3215–3218.

Edwards, G.E., Cantrell, C.A., Stephens, S., Hill, B., Goyea, O., Shetter, R.E., Mauldin, R.L., Kosciuch, E., Tanner, D.J., Eisele, F.E., 2003. Chemical ionization mass spectrometer instrument for the measurement of tropospheric HO_2 and RO_2. Analytical Chemistry 75, 4317–4327.

Eisele, F.L., 1989. Natural and anthropogenic negative ions in the troposphere. Journal Geophysical Research 94, 2183–2196.

Evans, M.J., Jacob, D.J., Atlas, E., Cantrell, C.A., Eisele, F., Flocke, F., Fried, A., Mauldin, R.L., Ridley, B.A., Wert, B., Talbot, R., Blake, D., Heikes, B., Snow, J., Walega, J., Weinheimer, A.J., Dibb, J., 2003. Coupled evolution of BrO_x–ClO_x–HO_x–NO_x chemistry during bromine-catalyzed ozone depletion events in the arctic boundary layer. Journal of Geophysical Research—Atmospheres 108 (D4).

Fehsenfeld, F.C., Howard, C.J., Schmeltekopf, A.L., 1975. Gas phase ion chemistry of HNO_3. Journal of Chemical Physics 61, 2835–2841.

Foster, K.L., Plastridge, R.A., Bottenheim, J.W., Shepson, P.B., Finlayson-Pitts, B.J., Spicer, C.W., 2001. The role of Br_2 and BrCl in surface ozone destruction at polar sunrise. Science 291 (5503), 471–474.

Hammer, C., Mayewski, P.A., Peel, D., Stuvier, P., 1997. Preface to the Greenland Summit ice cores special issue. Journal of Geophysical Research 102, 26,315–26,316.

Hausmann, M., Platt, U., 1994. Spectroscopic measurement of bromine oxide and ozone in the high Arctic during Polar Sunrise Experiment 1992. Journal of Geophysical Research 99, 25,399–25,413.

Helmig, D., Boulter, J., David, D., Birks, J.W., Cullen, N.J., Steffen, K., Johnson, B.J., Oltmans, S.J., 2002. Ozone and meteorological boundary-layer conditions at Summit, Greenland during 3–21 June 2000. Atmospheric Environment 36, 2595–2608.

Helmig, D, Ganzeveld, L., Butler, T., Oltmans, S.J., Ozone Atmosphere–Snow Gas Exchange, in review.

Helmig, D., Oltmans, S.J., Morse, T.O., Dibb, J.E., What is causing high ozone at Summit, Greenland. Atmospheric Environment, submitted for publication, this issue, doi:10.1016/j.atmosenv.2006.05.084.

Hönninger, G., Platt, U., 2002. Observations of BrO and it vertical distribution during surface ozone depletion at Alert. Atmospheric Environment 36, 2481–2489.

Honrath, R.E., Peterson, M.C., Guo, S., Dibb, J.E., Shepson, P.B., Campbell, B., 1999. Evidence of NO_x production within or upon ice particles in the Greenland snowpack. Geophysical Research Letters 26, 695–698.

Honrath, R.E., Lu, Y., Peterson, M.C., Dibb, J.E., Arsenault, M.A., Cullen, N.J., Steffen, K., 2002. Vertical fluxes of NO_x, HONO and HNO_3 above the snowpack at Summit, Greenland. Atmospheric Environment 36, 2629–2640.

Hutterli, M.A., Röthlisberger, R., Bales, R.C., 1999. Atmosphere-to-snow-to-firn transfer studies for HCHO at Summit, Greenland. Geophysical Research Letters 26, 1691–1694.

Hutterli, M.A., McConnell, J.R., Stewart, R.W., Jacobi, H.-W., Bales, R.C., 2001. Impact of temperature-driven cycling of hydrogen peroxide (H_2O_2) between air and snow on the planetary boundary layer. Journal of Geophysical Research 106, 15,395–15,404.

Hutterli, M.A., McConnell, J., Chen, G., Bales, R.C., Davis, D.D., Lenschow, D.H., 2004. Formaldehyde and hydrogen peroxide in air, snow and interstitial air at the South Pole. Atmospheric Environment 38, 5439–5450.

Jacobi, H.W., Frey, M.M., Hutterli, M.A., Bales, R.C., Schrems, O., Cullen, N.J., Steffen, K., Koehler, C., 2002. Measurement

of hydrogen peroxide and formaldehyde exchange between the atmosphere and surface snow at Summit, Greenland. Atmospheric Environment 36, 2619–2628.

Jones, A.E., Weller, R., Wolff, E.W., Jacobi, H.-W., 2000. Speciation and rate of photochemical NO and NO_2 production in Antarctic snow. Geophysical Research Letters 27, 345–348.

Lovejoy, E.R., Hanson, D.R., Huey, L.G., 1996. Kinetics and products of the gas-phase reaction of SO_3 with water. Journal of Physical Chemistry 100, 19911–19916.

Mauldin III, R.L., Eisele, F.L., Tanner, D.J., Kosciuch, E., Shetter, R., Lefer, B., Hall, S.R., Nowak, J.B., Buhr, M., Chen, G., Wang, P., Davis, D., 2001. Measurements of OH, H_2SO_4 and MSA at the South Pole during ISCAT. Geophysical Research Letters 28, 3629–3632.

Mauldin III, R.L., Cantrell, C.A., Zondlo, M.A., Kosciuch, E., Ridley, B.A., Weber, R., Eisele, F.E., 2003. Measurements of OH, H_2SO_4, and MSA during Tropospheric Ozone Production about the Spring Equinox (TOPSE). Journal of Geophysical Research 108, 8366–8384.

Mauldin III, R.L., Kosciuch, E., Henry, B., Eisele, F.L., Shetter, R., Lefer, B., Chen, G., Davis, D., Huey, G., Tanner, D., 2004. Measurements of OH, HO_2+RO_2, H_2SO_4 and MSA at the South Pole. Atmospheric Environment 38, 5423–5437.

Mayewski, P.A., Bender, M., 1995. The GISP-2 Ice core record—Paleoclimate highlights, U.S. National Report to the International Union of Geodesy and Geophysics 1991–1994. Reviews of Geophysics 33 (Part 2, Suppl. S), 1287–1296.

Peterson, M.C., Honrath, R.E., 2001. Observations of rapid photochemical destruction of ozone in snowpack interstitial air. Geophysical Research Letters 28, 511–514.

Ridley, B., Walega, J., Montzka, D., Grahek, F., Atla, E., Flocke, F., Stroud, V., Deary, J., Gallant, A., Boudries, H., Bottenheim, J., Anlauf, H., Worthy, D., Sumner, A.L., Shepson, P., 2000. Is the Arctic surface layer a source and sink of NO_x in winter/spring? Journal of Atmospheric Chemistry 36, 1–22.

Ryerson, T.B., Williams, E.J., Fehsenfeld, F.C., 2000. An efficient photolysis system for fast-response NO_2 measurements. Journal of Geophysical Research 105, 26,447–26,461.

Seibert, P., Frank, A., 2004. Source-receptor matrix calculation with a Lagrangian particle dispersion model in backward mode. Atmospheric Chemistry and Physics 4, 51–63.

Shetter, R.E., Müller, M., 1999. Photolysis frequency measurements using actinic flux spectroradiometry during the PEM-Tropics mission: instrumentation description and some results. Journal of Geophysical Research 104, 5647–5661.

Smith, S.C., Lee, J.D., Bloss, W.J., Johnson, G.P., Heard, D.E., 2005. Concentrations of OH and HO_2 radicals during NAMBLEX: measurements and steady state analysis. Atmospheric Chemistry and Physics Discussions 5, 12,403–12,464.

Sommariva, R., Bloss, W.J., Brough, N., Carslaw, N., Flynn, M., Haggerstone, A.-L., Heard, D.E., Hopkins, J.R., Lee, J.D., Lewis, A.C., McFiggans, G., Monks, P.S., Penkett, S.A., Pilling, M.J., Plane, J.M.C., Read, K.A., Saiz-Lopez, A., Rickard, A.R., Williams, P.I., 2005. OH and HO_2 chemistry during NAMBLEX: roles of oxygenates, halogen oxides and heterogeneous uptake. Atmospheric Chemistry and Physics Discussions 5, 10,947–10,996.

Stohl, A., Forster, C., Eckhardt, S., Spichtinger, N., Huntrieser, H., Heland, J., Schlager, H., Wilhelm, S., Arnold, F., Cooper, O., 2003. A backward modeling study of intercontinental pollution transport using aircraft measurements. Journal of Geophysical Research 108, 4370–4388.

Stohl, A., Forster, C., Frank, A., Seibert, P., Wotawa, G., 2005. Technical note: the Lagrangian dispersion model FLEXPART version 6.2. Atmospheric Chemistry and Physics 5, 2461–2474.

Stutz, J., Hebestreit, K., Alicke, B., Platt, U., 1999. Chemistry of halogen oxides in the troposphere: comparison of model calculations with recent field data. Journal of Atmospheric Chemistry 34 (1), 65–85.

Stutz, J., Kim, E.S., Platt, U., Bruno, P., Perrino, C., Febo, A., 2000. UV-visible absorption cross sections of nitrous acid. Journal of Geophysical Research 105, 14,585–14,592.

Swanson, A.L., Blake, N.J., Blake, D.R., Rowland, F.S., Dibb, J.E., 2002. Photochemically induced production of CH_3Br, CH_3I, C_2H_5I, ethane and propane within surface snow. Atmospheric Environment 36, 2671–2682.

Tanner, D.J., Jefferson, A., Eisele, F., 1997. Selected ion chemical ionization mass spectrometric measurement of OH. Journal of Geophysical Research 102, 6415–6425.

Viggiano, A.A., Perry, R.A., Albritton, D.L., Ferguson, E.E., Fehsenfeld, F.C., 1982. Stratospheric negative-ion reaction rates with H_2SO_4. Journal of Geophysical Research 87, 7340–7342.

von Glasow, R., von Kuhlman, R., Lawrence, M.G., Platt, U., Crutzen, P.J., 2004. Impact of reactive bromine chemistry in the troposphere. Atmospheric Chemistry and Physics 4, 2481–2497.

Yang, J., Honrath, R.E., Peterson, M.C., Dibb, J.E., Sumner, A.L., Shepson, P.B., Frey, M., Jacobi, H.-W., Swanson, A., Blake, N., 2002. Impacts of snowpack emission on deduced levels of OH and peroxy radicals at Summit, Greenland. Atmospheric Environment 36, 2523–2534.